Journal of Thermal Analysis and Calorimetry (2021) 143:1637–1654
https://doi.org/10.1007/s10973-020-09717-5

Effect of hybrid nanofluid on heat transfer performance of parabolic trough solar collector receiver

Recep Ekiciler[1] · **Kamil Arslan**[2] · **Oğuz Turgut**[1] · **Burak Kurşun**[3]

Received: 23 March 2020 / Accepted: 16 April 2020 / Published online: 23 April 2020

Abstract

In this study, three-dimensional heat transfer and flow characteristics of hybrid nanofluids under turbulent flow condition in a parabolic trough solar collector (PTC) receiver has been investigated. Ag–ZnO/Syltherm 800, Ag–TiO_2/Syltherm 800, and Ag–MgO/Syltherm 800 hybrid nanofluids with 1.0%, 2.0%, 3.0%, and 4.0% nanoparticle volume fractions are used as working fluids. Reynolds number is between 10,000 and 80,000. The temperature of the fluid is taken as 500 K. The C++ homemade code has been written for the nonuniform heat flux boundary condition for the outer surface of the receiver. Variations of thermal efficiency, heat transfer coefficient, friction factor, PEC number, Nusselt number, and temperature distribution are presented for three different types of hybrid nanofluids and four different nanoparticle volume fractions with different Reynolds numbers. Also, the graphs of the average percent increase according to Syltherm 800 are given for the working parameters. According to the results of the study, all hybrid nanofluids are found to provide superiority over the base fluid (Syltherm 800) with respect to heat transfer and flow features. Heat transfer augments with the growth of Reynolds number and nanoparticle volume fraction. Thermal efficiency, which is one of the important parameters for PTC, decreases with increasing Reynolds number and increases with the increasing volume fraction of nanoparticle. It is obtained that the most efficient working fluid for the PTC receiver is the Ag–MgO/Syltherm 800 hybrid nanofluid with 4.0% nanoparticle volume fraction.

Keywords Parabolic trough collector · Hybrid nanofluid · Thermal efficiency · Solar irradiance · Nonuniform heat flux

List of symbols

A	Area (m^2)
k	Turbulent kinetic energy ($m^2\ s^{-2}$)
C_p	Specific heat ($J\ kg^{-1}\ K^{-1}$)
u_i, u_j	Averaged velocity components ($m\ s^{-1}$)
x, y, z	Cartesian coordinates (m)
P	Pressure (Pa)
$-\rho\overline{u_i'u_j'}$	Reynolds stress ($N\ m^{-2}$)
x_i, x_j	Spatial coordinates (m)
T	Temperature (K)
k_r	Thermal conductivity of the receiver material ($W\ m^{-1}\ K^{-1}$)
f	Friction factor
Re	Reynolds number
Nu	Nusselt number
h	Heat transfer coefficient ($W\ m^{-2}\ K^{-1}$)
u', v', w'	Fluctuations of velocity ($m\ s^{-1}$)
G_k	Generation of turbulent kinetic energy due to mean velocity gradients ($kg\ m^{-1}\ s^{-3}$)
C_1, C_2, C_μ	Turbulent model constants
S_{ij}	Rate of linear deformation tensor (s^{-1})
S	Modulus of the mean rate of strain tensor (s^{-1})
u, v, w	Velocity components ($m\ s^{-1}$)
q''	Heat flux ($W\ m^{-2}$)
I	Direct normal irradiance ($W\ m^{-2}$)
d	Receiver diameter (m)
ΔP	Pressure difference (Pa)
L	Length of the receiver (m)
$\dot{m}$	Mass flow rate ($kg\ s^{-1}$)
Pr	Prandtl number

Greek letter

θ	Circumferential angle of receiver (°)
θ_r	Rim angle (°)

✉ Recep Ekiciler
recepekiciler@gazi.edu.tr

[1] Mechanical Engineering Department, Gazi University, 06570 Ankara, Turkey

[2] Mechanical Engineering Department, Karabuk University, 78050 Karabük, Turkey

[3] Mechanical Engineering Department, Amasya University, 05100 Amasya, Turkey

ρ	Density (kg m^{-3})
μ	Viscosity (Pa s)
δ_{ij}	Kronecker delta
λ	Fluid thermal conductivity (W m^{-1} K^{-1})
$\sigma_{h,t}$	Turbulent Prandtl number for energy
μ_t	Eddy viscosity (Pa s)
ε	Turbulent dissipation rate (m^2 s^{-3})
σ_k	Turbulent Prandtl number for k
σ_ε	Turbulent Prandtl number for ε
ν	Kinematic viscosity (m^2 s^{-1})
η	Turbulence model parameter
η_{ter}	Thermal efficiency
ϕ	Nanoparticle volume fraction

Subscript

p	Aperture
i	Inlet
f	Fluid
eff	Effective
hnf	Hybrid nanoparticle
p1, p2	Nanoparticle
i, j, k	Spatial indices
inner	Receiver inner surface
w	Wall
b	Bulk
o	Outlet

Superscript

′	Fluctuation from average value
–	Time-averaged value

Introduction

Solar energy is the most abundant, cleanest, and cheapest energy in the world. Its utilization is the encouraging approach for challenging the substantial problems such as global warming, fossil fuel depletion, and energy requirement [1]. Concentrated solar power (CSP) technology is a promising method for generating electricity and heating fluids. In medium temperature ranges, parabolic trough solar collectors (PTC) is the most suitable selection in the CSP technology method [2]. PTC is used in various applications including chemical process, heating domestic water, generating electricity, refrigeration, and desalination [3].

Recently, many studies related to enhancing the thermal performance of PTC have been published by using nanofluid, inserts placed in the receiver such as turbulator and fin. One of the thermal performance enhancement techniques is the utilization of nanofluid as a working fluid. Nanofluid, which is found in 1995 by Choi [4], is prepared by dispersing nanoparticles in the base fluid such as water, oil, and ethylene glycol, etc. It provides two advantages to the base fluid: The first one is that while the nanofluid is composed, nanoparticle having higher thermal conductivity is preferred in terms of obtaining the nanofluid with higher thermal conductivity in comparison with the base fluid. The added nanoparticles expand the surface area of the conventional fluid and allow it to have more heat capacity [4]. This causes the thermal conductivity coefficient of the nanofluid to be high [5]. The last one is to create the nanofluid with higher density. The higher density contributes to higher density-specific heat capacity. This provides to transfer extra heat [6]. Nanofluids are used in many applications such as heat sinks [7], carbon nanotubes [8–11], solar energy systems [12], and automotive industry [13].

In solar collectors, especially PTC, a few studies regarding heat transfer applications with nanofluid have been performed. Amina et al. [14] analyzed numerically the thermal performance in PTC by using various nanofluids (Al_2O_3/Dowtherm-A, SiC/Dowtherm-A, C/Dowtherm-A, and Cu/Dowtherm-A) and longitudinal fins with a rectangular and triangular shape. They tried to understand the effect of types of nanoparticle and fin geometry on thermal performance under turbulent flow conditions. The temperature was kept constant at 573 K. Nonuniform heat flux, which is got with Monte Carlo Ray Tracing (MCRT) method, was subjected to the outer wall of the receiver. They noticed that the nanofluid with metallic nanoparticles shows superior thermal performance than the nonmetallic nanoparticles. The value of Nusselt number with fins is between 1.3 and 1.8 times greater with changing of the Reynolds number than the plain receiver. The friction factor with the nanofluid and triangular fin is approximately two times greater than the plain receiver. Bretado de los Rios et al. [15] performed an experimental study on the PTC by using water-based nanofluid including between 1.0 and 3.0% Al_2O_3 nanoparticles. In addition, they investigated the effect of incident angle on collector efficiency. It was revealed that thermal performance with the nanofluid is always greater than the water for all incident angles. The incident angle is a substantial factor for the efficiency of PTC. It is inversely proportional to the thermal efficiency of PTC. Using nanofluid having 3.0% nanoparticle volume fraction presents about 10.0% increment in thermal performance. For the same inlet temperature, the outlet temperature of nanofluid is hotter than the water temperature. They understood that the nanofluid is encouraging working fluid for the PTCs. Ghasemi and Ranjbar [16] investigated numerically the influence of the working fluid of Al_2O_3/water and CuO/water nanofluid on the efficiency of the PTC. Different heat flux was exposed to the bottom and top half periphery of the absorber. Inlet temperature was assumed constant at 320 K. The results indicated that by adding more nanoparticle volume fraction, the heat transfer rises for the nanofluids. Using CuO/water nanofluid, the enhancement of the heat transfer coefficient is reached up to 35%. Kaloudis et al. [17] investigated a three-dimensional numerical turbulent mixed convective heat transfer problem with the two-phase approach and in LS2-module PTC exposed nonuniform heat flux by using Al_2O_3/Syltherm 800 nanofluid having different nanoparticle volume fraction (0.0–4.0%). It was found that there is a 10% increment in system efficiency by using the highest nanoparticle concentration. Khakrah et al. [18] numerically examined the thermal performance of Al_2O_3/Synthetic oil nanofluid-based PTC. They studied the absorber tube having nonuniform heat flux distribution to find the influence of nanoparticle concentration, wind velocity, and inlet temperature on the overall collector efficiency. MCRT technique was utilized to determine the nonuniform heat flux providing more precise results. The working fluid properties are assumed to depend on inlet temperature and nanoparticle concentration. The outcomes of the study indicated that using nanofluid with 5.0% nanoparticle concentration shows 14.3% overall efficiency in comparison with the synthetic oil. Moreover, they noticed that the effect of wind velocity on efficiency could be neglected. Mwesigye et al. [19] investigated a three-dimensional numerical study to find optimal Al_2O_3/Syltherm 800 nanofluid turbulent flow condition of PTC via entropy minimization method. They used thermal governing and thermodynamic equations to solve the problem. Many parameters such as nanoparticle concentration (0.0–8.0%), inlet temperature (350–600 K), and Reynolds number (3560–1,151,000) were studied. Local entropy generation rate, Bejan number, collector thermal efficiency, heat transfer, and friction factor were presented. They declared that the thermal efficiency of PTC with nanofluid can be augmented to 76% by adding 8.0% nanoparticle concentration. They suggested an optimal Reynolds number correlation with respect to nanoparticle concentration and Prandtl number. By adding more nanoparticle to the base fluid, the value of the optimal Reynolds number decreases. Mwesigye et al. [20] studied a numerical study Cu/Therminol VP-1 nanofluid-based PTC of entropy generation study and thermal performance. They subjected real-like heat flux to the receiver obtained from the MCRT method. They studied the effects of several parameters including inlet temperature, nanoparticle volume fraction, and Reynolds number on pressure drop, thermal performance, heat transfer coefficient, entropy generation rate, and Bejan number. The results showed that using the highest nanoparticle concentration (6.0%) thermal efficiency goes up to 32%. At the same time, the utilization of nanofluid enhances thermodynamic performance. Entropy generation in the receiver decreases with increasing nanoparticle concentration at some defined Reynolds number.

Recently, a new promising fluid, called hybrid nanofluid, has been used to enhance the heat transfer in thermal applications [21–23]. Hybrid nanofluids are expected to decline in the price of the single type nanofluid by the researchers [24]. They can consist of two or more than two unsimilar nanoparticles, which can be either nanocomposite or in the mixture. They considered a possible heat transfer fluid instead of using single type nanofluid in order to enhance the thermophysical properties of single type nanofluid [25]. Minea [26] investigated a three-dimensional numerical study of turbulent forced convection heat transfer in a tube by using hybrid nanofluid (Al_2O_3–SiO_2/water, Al_2O_3–TiO_2/water) and single-phase approach. She changed the nanoparticle concentration to see heat transfer enhancement of hybrid nanofluid. Moreover, the performance of the nanofluid with single nanoparticle compared at the same conditions. It was noticed that the heat transfer coefficient of 2.5% Al_2O_3–1.5% SiO_2/water hybrid nanofluid has the highest value in comparison with pure water. Moghadassi et al. [27] numerically investigated the effects of Al_2O_3/water nanofluid and Al_2O_3–Cu/water hybrid nanofluid with constant nanoparticle concentration of 0.1% in tube exposed to uniform heat flux. They analyzed the performance evaluation criterion (PEC), pressure drop, and Nusselt number. The results of the study declared that the Nusselt number obtained from the single-phase method is enhanced by 13.46% and 4.73% when compared pure water and the single type nanofluid, respectively. They noticed that looking at this result, adding Cu nanoparticle augments an extra 5.0% heat transfer performance. They also suggested two correlations as a function of the Reynolds number and Prandtl number regarding friction factor and Nusselt number. Chamkha et al. [28] focused two-dimensional numerical unsteady natural convective heat transfer in a cavity via single-phase approach. They investigated the influence of the water-based hybrid nanofluid with Al_2O_3 and Cu nanoparticles on natural convection. Several parameters, including Rayleigh number, dimensionless time, and nanoparticle concentration, etc., were performed. It was obtained that the hybrid nanofluid is dominant for the high Rayleigh numbers. The detailed review about hybrid nanofluid pertaining to its characterization, preparation, thermophysical properties and usage area in the applications can be found in Refs. [25, 29, 30].

In PTCs, the utilization of the hybrid nanofluid is not extensive due to the new promising heat transfer fluid. Minea and El-Maghlany [31] presented both a review of hybrid nanofluids and a two-dimensional numerical simulation of hybrid nanofluid (Ag–MgO/water, GO–Co_3O_4/60EG:40 W, Cu–Al_2O_3/water)-based PTC with uniform heat flux in a laminar regime by using single-phase approach. They studied thermal efficiency, heat transfer and hydraulic performance of the PTC. The outcomes of the study declared that using the Cu–Al_2O_3/water hybrid nanofluid decreases the heat transfer performance due to the higher viscosity in comparison with the water. However, Ag–MgO/water hybrid nanofluid having 2.0% nanoparticle concentration enhances the heat transfer up to 14.0%. Bellos and Tzivanidis [32] compared the performance of the single type nanofluid (3.0 vol% Al_2O_3/Syltherm 800 and 3.0 vol% TiO_2/Syltherm 800) and hybrid nanofluid (1.5 vol% Al_2O_3–1.5 vol% TiO_2/Syltherm 800) in a PTC with uniform heat flux distribution of 1000 W m^{-2} for the different inlet temperatures (300–600 K) by using Engineering Equation Solver (EES). They presented thermal efficiency, Nusselt number, and improvement of heat transfer coefficient, exergy efficiency as a function of inlet temperature. They revealed that the thermal efficiency with hybrid nanofluid has 2.2 times the great performance in comparison with base oil.

As can be seen from the literature, studies using hybrid nanofluids represent the minority. Especially in PTCs which are renewable energy applications, the use of hybrid nanofluid is very limited. Studies have been carried out with parameters such as two-dimensional, laminar conditions. In this study, unlike the studies in the literature, three-dimensional and turbulent flow conditions using three different hybrid nanofluid (Ag–ZnO/Syltherm 800, Ag–TiO_2/Syltherm 800, and Ag–MgO/Syltherm 800) thermal and hydrodynamic features are investigated using the receiver of LS-2 type PTC. While forming the hybrid nanofluid, all nanoparticles are added at 50–50%. This study is believed to fill an important gap in the literature on heat transfer performance and flow characteristics of hybrid nanofluids in PTCs. The selection of hybrid nanoparticles has been considered for the following reasons: (1) High permeability and good electrical conductivity properties are also the preferred reasons for using ZnO nanoparticle [33]. (2) The purpose of using silver metal is to produce a more efficient heat transfer fluid by making use of its significantly higher thermal conductivity. (3) The high level of stability of TiO_2 is advantageous when used in nanofluid [34]. (4) MgO nanoparticles can be more easily suspended than other metal oxides and are less likely to precipitate and sediment [35]. The volume fractions of nanoparticles volume fractions are added to the base fluid are 1.0%, 2.0%, 3.0% and 4.0%. The Reynolds number is between 10,000 and 80,000. Nusselt number, friction factor, heat transfer coefficient, PEC number, and thermal efficiencies are analyzed using the above-mentioned parameters. Temperature distribution inside the PTC is also provided.

Physical model

The PTCs consist of a reflective surface with a parabolic shape and a receiver. This surface allows the sun's rays to concentrate on the receiver. In the numerical study, the rim angle (θ_r) of the collector is 70° and the total aperture area ($A_p = W \times L$) is 39 m^2 [36]. The LS-2 parabolic trough solar collector shown in Fig. 1 has been examined. The geometric parameters and material properties of the receiver are given in Table 1. The material of the receiver is 316L steel.

Numerical study

Mathematical model

The numerical study is carried out under three-dimensional, steady-state and turbulent flow conditions with single-phase approach. Three different hybrid nanofluids are used: Ag–ZnO/Syltherm 800, Ag–TiO_2/Syltherm 800,

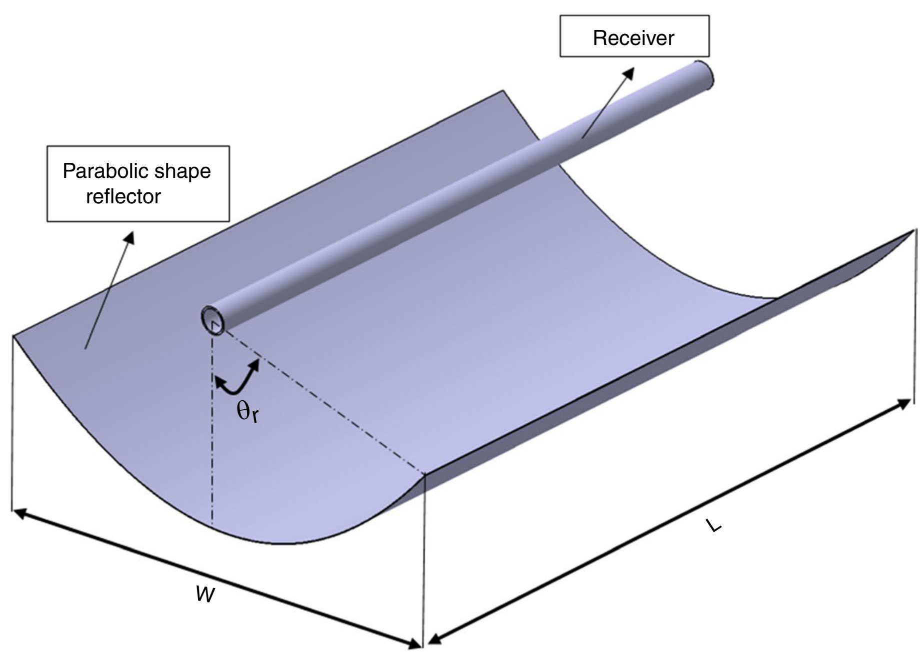

Fig. 1 View of parabolic trough collector and its components

Table 1 LS-2 type receiver structural and material properties

Receiver geometrical dimensions [37]		
Outer diameter/m	Inner diameter/m	Length of the receiver/m
0.7	0.66	7.8
Receiver material properties [38]		
k_r/W m^{-1} K^{-1}	C_p/J kg^{-1} K^{-1}	ρ/kg m^{-3}
24.92	502.48	8030

and Ag–MgO/Syltherm 800. During the study, it is assumed that the fluids are incompressible, Newtonian and convective properties are not changed. It is also assumed that the thermophysical properties of the fluids do not change with temperature. This means that the buoyancy effect is neglected. Many studies that ignore the buoyancy effect can be seen [39–41]. These studies are compared with numerical and experimental studies, the difference between the numerical results and the experimental results is very small. It is assumed that the nanoparticles homogeneously disperse in the base fluid.

Governing equations

In the light of the above assumptions governing equations in three-dimensional and turbulent flow conditions are as follows [42]:

Continuity:

$$\frac{\partial(\rho u_i)}{\partial x_i} = 0 \tag{1}$$

Momentum:

$$\frac{\partial}{\partial x_i}(\rho u_i u_j) = -\frac{\partial P}{\partial x_i} + \frac{\partial}{\partial x_j}\left[\mu\left(\frac{\partial u_i}{\partial x_j} + \frac{\partial u_j}{\partial x_i}\right) - \frac{2}{3}\mu\frac{\partial u_i}{\partial x_i}\delta_{ij} - \rho\overline{u'_j u'_j}\right] \tag{2}$$

Energy:

$$\frac{\partial}{\partial x_j}(\rho u_j C_p T) = -\frac{\partial}{\partial x_i}\left(\lambda\frac{\partial T}{\partial x_j} + \frac{\mu_t}{\sigma_{h,t}}\frac{\partial(C_p T)}{\partial x_j}\right) + u_j\frac{\partial P}{\partial x_j} + \left[\mu\left(\frac{\partial u_i}{\partial x_j} + \frac{\partial u_j}{\partial x_i}\right) - \frac{2}{3}\mu\frac{\partial u_i}{\partial x_i}\delta_{ij} - \rho\overline{u'_i u'_j}\right]\frac{\partial u_i}{\partial x_j} \tag{3}$$

where $-\rho\overline{u'_i u'_j}$ are the Reynolds stresses, u_i and u_j are the time-averaged velocity for i and j directions. Time-averaged temperature, fluid thermal conductivity, density, turbulent Prandtl number for energy, turbulent viscosity and time-averaged pressure are stated as T, λ, ρ, $\sigma_{h,t}$, μ_t and P, respectively.

Reynolds stresses, including velocity gradients, are expressed as follows due to the Boussinesq hypothesis [43]:

$$-\rho\overline{u'_i u'_j} = \mu_t\left(\frac{\partial u_i}{\partial x_j} + \frac{\partial u_j}{\partial x_j}\right) - \frac{2}{3}\left(\rho k + \mu_t\frac{\partial u_k}{\partial x_k}\right)\delta_{ij} \tag{4}$$

where the turbulent kinetic energy is defined as k, which is given in the following form,

$$k = \frac{1}{2}\left(\overline{u'^2} + \overline{v'^2} + \overline{w'^2}\right) \tag{5}$$

As a turbulence model for industrial fluid problems, the k–ε turbulence model is generally used in order to give fast and accurate results [43, 44]. In the numerical study, solutions have been realized with realizable k–ε turbulence model. For this model, two new equations, turbulent dissipation rates (ε) and transport of turbulence kinetic energy (k), should be considered.

k equation:

$$\frac{\partial}{\partial x_j}(\rho k u_j) = \frac{\partial}{\partial x_i}\left[\left(\mu + \frac{\mu_t}{\sigma_k}\right)\frac{\partial k}{\partial x_j}\right] + G_k - \rho\varepsilon \tag{6}$$

ε equation:

$$\frac{\partial}{\partial x_j}(\rho\varepsilon u_j) = \frac{\partial}{\partial x_i}\left[\left(\mu + \frac{\mu_t}{\sigma_\varepsilon}\right)\frac{\partial\varepsilon}{\partial x_j}\right] + \rho C_1 S\varepsilon - \rho C_2\frac{\varepsilon^2}{k + \sqrt{\nu\varepsilon}} \tag{7}$$

Turbulent Prandtl number is expressed as σ_k and σ_ε regarding k and ε in Eqs. (6) and (7).

The production of turbulent kinetic energy is called G_k and calculated from the following equation.

$$G_k = \rho\overline{u'_i u'_j}\frac{\partial u_i}{\partial x_i} \tag{8}$$

When the production of turbulent kinetic energy (G_k) is evaluated with Eq. (4), G_k may be stated as the following equation.

$$G_k = \mu_t S^2 \tag{9}$$

where S is defined as modulus of the mean rate of the strain tensor.

Equation (10) represents the turbulent viscosity.

$$\mu_t = \rho C_\mu \frac{k^2}{\epsilon} \tag{10}$$

Constants for the realizable k–ε turbulent model are expressed below,

$$C_1 = \max\left[0.43, \frac{\eta}{\eta+5}\right], \quad \eta = S\frac{k}{\varepsilon}, \quad S \equiv \sqrt{2S_{ij}S_{ij}}$$
$$C_2 = 1.9, \quad \sigma_k = 1, \quad \sigma_\varepsilon = 1.2$$

The detailed calculation of C_μ is presented in Ref. [43].

Thermophysical properties of hybrid nanofluid

The thermophysical properties of the nanoparticles and base fluid Syltherm 800 are given in Table 2.

The hybrid nanofluid density, heat capacitance, dynamic viscosity, and thermal conductivity are determined from the below equations.

The effective density [46]:

$$\rho_{eff} = \phi\rho_{hnp} + (1-\phi)\rho_f \tag{11}$$

The heat capacitance [47]:

$$\left(\rho C_p\right)_{eff} = \phi\left(\rho C_p\right)_{hnp} + (1-\phi)\left(\rho C_p\right)_f \tag{12}$$

The dynamic viscosity [48]:

$$\mu_{eff} = \frac{\mu_f}{(1-\phi)^{2.5}} \tag{13}$$

The thermal conductivity [49]:

$$\lambda_{eff} = \lambda_f \frac{\left(\lambda_{hnp} + 2\lambda_f\right) - 2\phi\left(\lambda_f - \lambda_{hnp}\right)}{\left(\lambda_{hnp} + 2\lambda_f\right) + \phi\left(\lambda_f - \lambda_{hnp}\right)} \tag{14}$$

ρ_{hnp}, C_{phnp}, λ_{hnp} and ϕ are obtained from the following equations [47] :

Table 2 Properties of nanoparticles and base fluid [25, 30, 45]

	ρ/kg m^{-3}	C_p/J kg^{-1} K^{-1}	λ/W m^{-1} K^{-1}	μ/Pa s
Syltherm 800	747.2	1962	0.0961	0.00084
Ag	10,500	236	426.77	–
ZnO	5630	494	27.196	–
TiO_2	4250	686	8.786	–
MgO	3580	921	69.036	–

$$\rho_{hnp} = \frac{\rho_{p1}\phi_{p1} + \rho_{p2}\phi_{p2}}{\phi} \tag{15}$$

$$C_{p\,hnp} = \frac{C_{p\,p1}\phi_{p1} + C_{p\,p2}\phi_{p2}}{\phi} \tag{16}$$

$$\lambda_{hnp} = \frac{\lambda_{p1}\phi_{p1} + \lambda_{p2}\phi_{p2}}{\phi} \tag{17}$$

$$\phi = \phi_{p1} + \phi_{p2} \tag{18}$$

Boundary conditions

- Constant and uniform velocity and temperature for receiver inlet

  $u = 0, \quad v = 0, \quad w = w_i, \quad T = T_i = 500\,\mathrm{K}.$

- The pressure is equal to atmospheric pressure at the outlet of the receiver

  $P = P_{gage} = 0$

- Nonuniform heat flux is applied to the exterior of the receiver to obtain more realistic results.
- Nonuniform heat flux profile has been get using Monte Carlo Ray Tracing (MCRT) method [50]. In this study, homemade C++ code which is suitable for nonuniform heat flux profile obtained by using MCRT is written and the resulting heat flux is compared with the profile in Fig. 2a. As shown in the figure, these two heat flux profiles have a good fit. Figure 2a shows the local concentration ratio (LCR) values. The local concentration ratio is found by the formula LCR = $\frac{q''_w}{I}$. Here I is direct normal irradiance and I = 1000 W m^{-2}. Figure 2b shows the heat flux distribution on the outside surface of the receiver.
- The radiation from the outer surface of the receiver is ignored because heat transfer performance is analyzed in the receiver as in the Refs. [50, 51].
- No-slip conditions are applied to all solid surfaces.

  $u = 0, \quad v = 0 \quad w = 0.$

Numerical solution

Numerical solutions are obtained by solving continuity, momentum and energy equations with boundary conditions. These solutions are realized with the commercial ANSYS 19.1 package program. The receiver geometry is drawn with ANSYS Design Modeler, the mesh structure

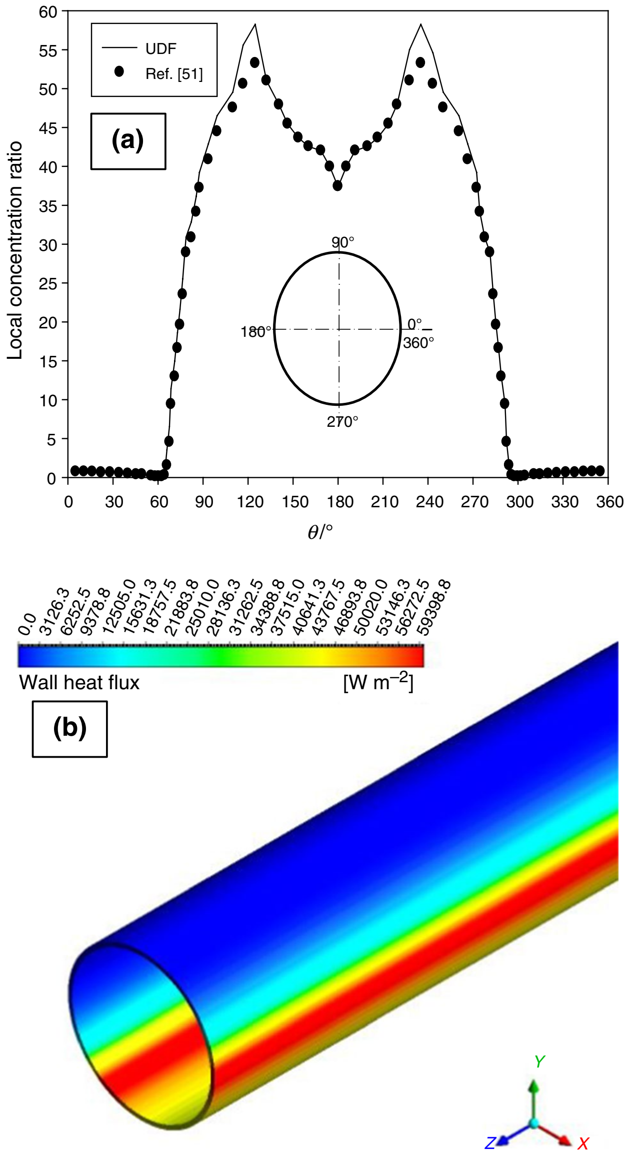

Fig. 2 **a** Validation of local concentration ratio and **b** distribution of heat flux

of the receiver is made in ANSYS Meshing, and governing equations are determined in ANSYS Fluent.

ANSYS Fluent makes the solution by using the finite volume method. The SIMPLE algorithm is utilized for the solution of pressure–velocity coupling. The second-order upwind scheme is adopted to discrete the algebraic equations. Enhanced wall treatment (EWT) technique is used to obtain better results in areas close to the recipient walls [43]. The numerical solutions are done until the residual of the continuity equation, momentum equations, energy equation, turbulent kinetic energy rate, and turbulent kinetic energy values are less than 10^{-8}.

Data reduction

In this study, the influences of hybrid nanofluids on heat and flow characteristics are analyzed. During this analysis, the Reynolds number, Nusselt number, friction factor, heat transfer coefficient, and thermal efficiency expressions are calculated as follows:

Effective Reynolds number is calculated by Eq. (19) [42],

$$\mathrm{Re}_{\mathrm{eff}} = \frac{\rho_{\mathrm{eff}} w_{\mathrm{ieff}} d_{\mathrm{inner}}}{\mu_{\mathrm{eff}}} \tag{19}$$

where ρ_{eff} is effective fluid density, w_{ieff} is effective fluid inlet velocity, d_{inner} is the receiver inner diameter, and μ_{eff} is effective fluid dynamic viscosity.

Equation (20) presents the determination of effective convection heat transfer coefficient [42],

$$h_{\mathrm{eff}} = \frac{q''_{\mathrm{w}}}{\left(T_{\mathrm{w\,inner}} - T_{\mathrm{b}}\right)} \tag{20}$$

where q''_{w} is heat flux on the outer receiver surface, $T_{\mathrm{w\,inner}}$ is the receiver inner wall temperature, and T_{b} is bulk temperature which is equal to $\left(T_{\mathrm{i}} + T_{\mathrm{o}}\right)/2$. T_{o} is fluid outlet temperature.

Effective Nusselt number is stated as in Eq. (21) [42],

$$\mathrm{Nu}_{\mathrm{eff}} = \frac{h_{\mathrm{eff}} d_{\mathrm{inner}}}{\lambda_{\mathrm{eff}}} \tag{21}$$

where λ_{eff} is effective fluid thermal conductivity.

Effective friction factor is obtained from Eq. (22) [42],

$$f_{\mathrm{eff}} = \frac{\Delta P\left(d_{\mathrm{inner}}/L\right)}{\rho_{\mathrm{eff}}\left(w_{\mathrm{ieff}}\right)^2/2} \tag{22}$$

where ΔP is pressure difference and L is the length of the receiver.

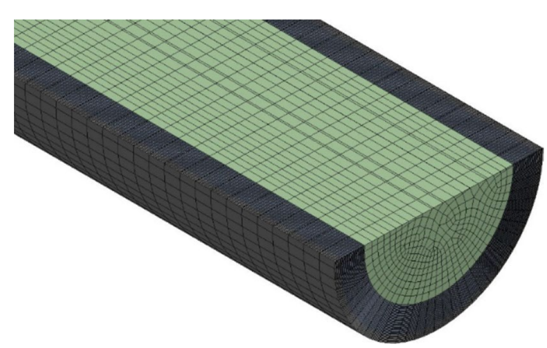

Fig. 3 View of lateral and cross-sectional mesh distribution

Thermal efficiency of the receiver is evaluated with Eq. (23) [31],

$$\eta_{\text{ter}} = \frac{\left(\dot{m}C_{\text{p}}\text{d}T\right)_{\text{eff}}}{IA_{\text{p}}} \tag{23}$$

where $\dot{m}$ is mass flow rate, C_p is specific heat of the working fluid, dT is temperature gradient which is expressed as the difference between the average outlet temperature ($T_{\text{o @L}}$) and bulk temperature. I is direct normal irradiance and A_p is collector aperture area.

Performance evaluation criterion (PEC) is a dimensionless number representing heat transfer and hydraulic performance of thermal applications. It is calculated by the following formula [52]:

$$\text{PEC} = \frac{\left(\text{Nu}_{\text{hnf}}/\text{Nu}_{\text{bf}}\right)}{\left(f_{\text{hnf}}/f_{\text{bf}}\right)^{\frac{1}{3}}} \tag{24}$$

Here the subscript of hnf and bf representS the hybrid nanofluid and base fluid, respectively.

Verification of results of the simulation

Checking of grid independence

In this study, the hexahedral mesh structure is used as can be seen from Fig. 3. Mesh concentration is intensified in the inner walls of the receiver. In the near-wall region, the value of y^+ is approximately ensured 1. In the figure, the outermost

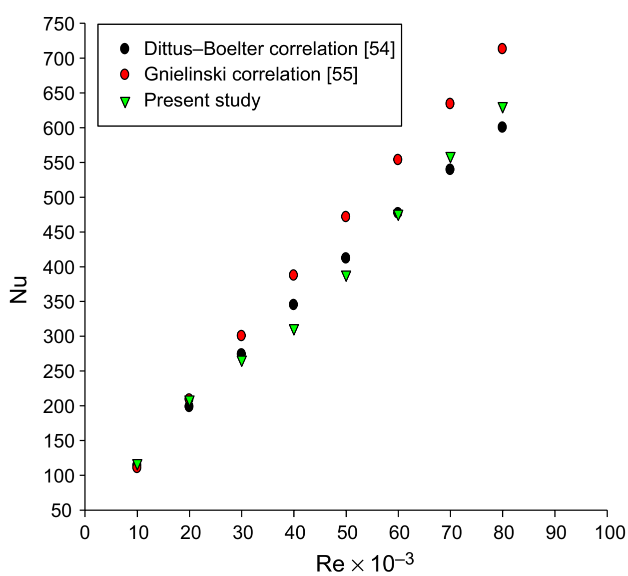

Fig. 4 Validation of Nusselt number of Syltherm 800 with the literature correlations

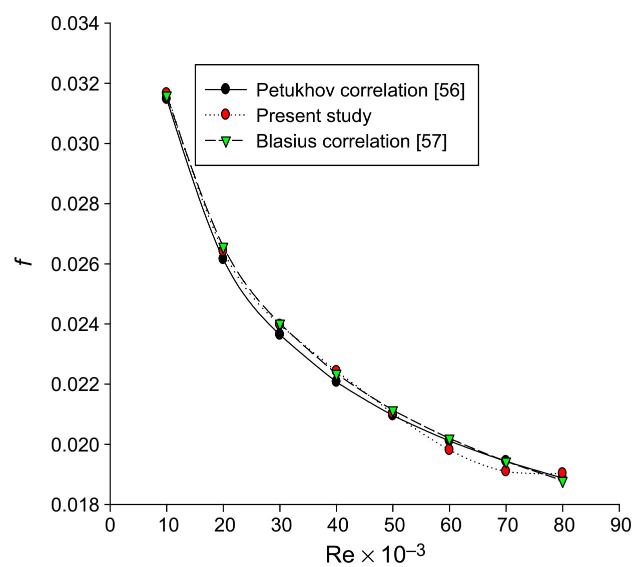

Fig. 5 Validation of friction factor of Syltherm 800 with the literature correlations

Table 3 Results of grid-independent checking

Grid number	h/W m^{-2} K^{-1}	Deviation/%	T_w/K	Deviation/%	f/–	Deviation/%
52697	1500.5830	–	1024.6720	–	0.026846	–
106362	1295.6240	13.6586	802.4830	21.68391	0.025675	4.361916
222846	1066.8730	17.6557	667.1480	16.86453	0.023325	9.154430
354231	978.6820	8.26631	590.6830	11.46147	0.02137	8.380851
468378	945.9520	3.34429	542.8490	8.098083	0.020367	4.692136
549125	929.1670	1.7744	530.3150	2.308929	0.019974	1.928601
694268	921.6793	0.80585	529.2870	0.193847	0.019255	3.602629
787400 (selected)	918.9510	0.29601	528.3920	0.169095	0.019023	1.203343
876389	917.6540	0.14114	527.6780	0.135127	0.018962	0.320139
1025978	916.5870	0.11627	527.5690	0.020657	0.018921	0.216748
1250943	916.8790	0.031857	527.4670	0.019334	0.018918	0.015855
1527546	916.7354	0.01566	527.3890	0.01478	0.018914	0.02114

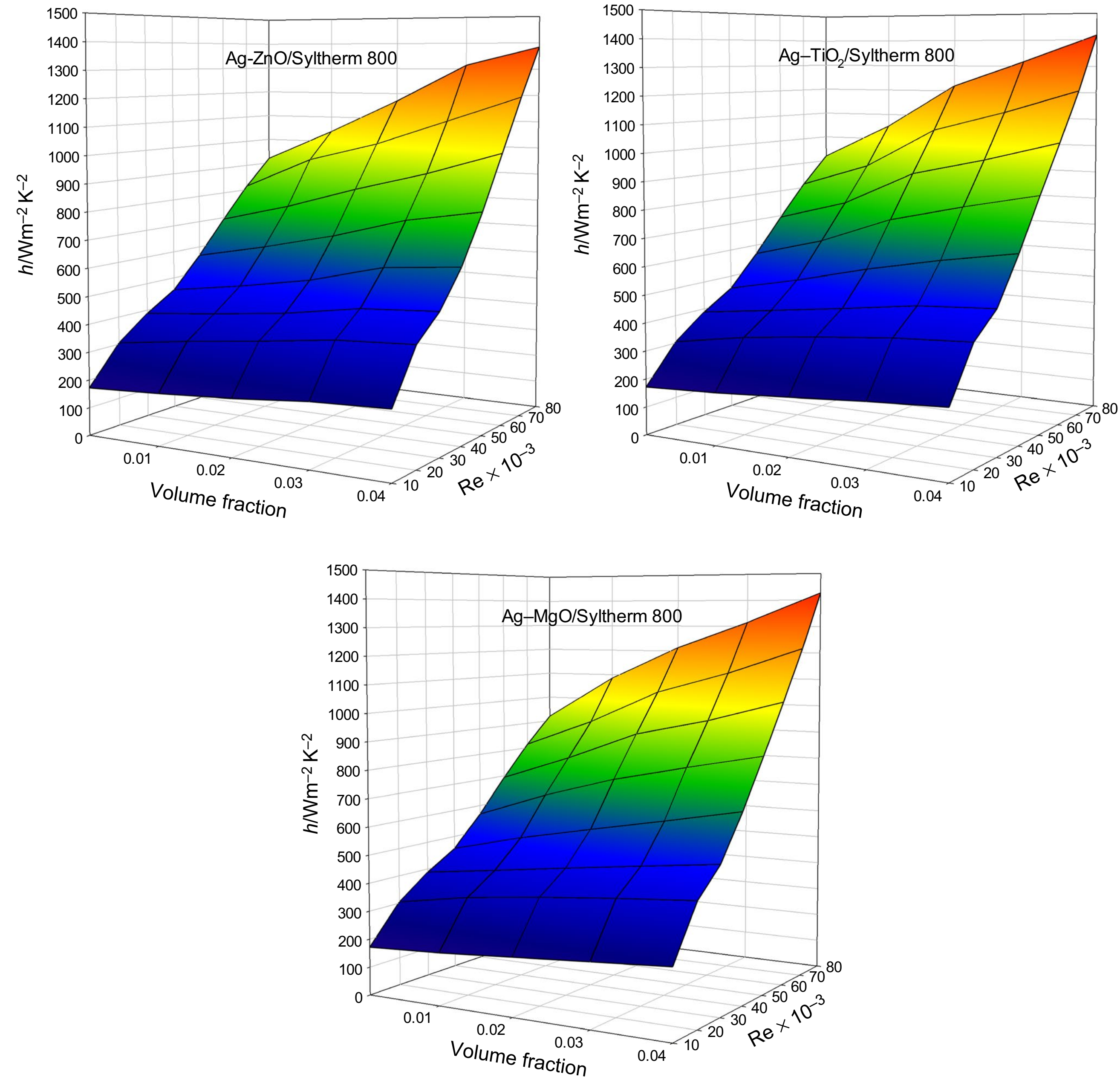

Fig. 6 Distribution of convection heat transfer coefficient for different hybrid nanofluid types as a function of nanoparticle volume fraction and Reynolds number

brown part shows the receiver wall made of steel. The other areas show the flow area.

In order to test the independence of the numerical results from the number of mesh, the number of mesh is increased, and the convection heat transfer coefficient, wall temperature, and friction factor values are obtained at the highest Reynolds number (Re = 80,000) and for Syltherm 800. These values are given in Table 3 for 11 different mesh numbers. The error percentages for each variable are found in the table, and it is noticed that the change in convection heat transfer coefficient, wall temperature, and friction factor values is very small especially after 787,400 mesh number. Accordingly, the optimum number of meshes is found to be 787,400 for faster and more accurate results.

Checking the results of the study with literature

The Nusselt number of the base fluid Syltherm 800 is compared with the correlation and Dittus–Boelter (Eq. 25) and Gnielinski (Eq. 26). The maximum deviation of the present study's Nusselt number from the Dittus–Boelter and Gnielinski correlations is 5.70% and 15.62%, respectively. Figure 4 shows that the Nusselt number values are appropriate. When correlation is used in industrial applications, the error is allowed up to 20% [51, 53].

Dittus–Boelter correlation [54]:

$$\mathrm{Nu} = 0.023\mathrm{Re}^{0.8}\,\mathrm{Pr}^{0.4} \tag{25}$$

Gnielinski correlation (for $0.5 \le \mathrm{Pr} \le 2000$ and $3000 \le \mathrm{Re} \le 5{,}000{,}000$) [55]:

$$\mathrm{Nu} = \frac{\left(f/8\right)(\mathrm{Re} - 1000)\,\mathrm{Pr}}{1 + 12.7\left(f/8\right)^{0.5}\left(\mathrm{Pr}^{2/3} - 1\right)} \tag{26}$$

In Fig. 5, the friction factor of the base fluid Syltherm 800 is compared with the correlations of Petukhov (Eq. 27) and Blasius (Eq. 28). It is determined that the maximum deviation of the present study's friction factor from the Petukhov and Blasius correlations is 1.74% and 1.56%, respectively. Again, the results are consistent with each other.

Petukhov correlation [56]:

$$f = (0.790\ln\mathrm{Re} - 1.64)^{-2} \tag{27}$$

Blasius correlation (for $4000 \le \mathrm{Re} \le 100{,}000$) [57]:

$$f = 0.316\mathrm{Re}^{-0.25} \tag{28}$$

As a result, when looking at Figs. 4 and 5, it is understood that the present numerical code can be used for simulating this physical problem.

Results and discussion

In this section, the heat transfer and flow characteristics of the receiver are examined by combining the effect of different hybrid nanofluids with different parameters. Figure 6 shows the effect of different hybrid nanofluids and Syltherm 800 on the convection heat transfer coefficient. These figures are plotted with respect to the Reynolds number and nanoparticle volume fraction of different hybrid nanofluids. When the graphs are examined, it is observed that the convection heat transfer coefficient increases as the volume fraction of nanoparticles increases in all hybrid nanofluids. This can be attributed to the fact that the fraction of nanoparticles changes the thermophysical properties of the base fluid and increases the convective heat transfer performance. For example, at the Reynolds number 80,000, the convective heat transfer coefficient of the increased nanoparticle volume fraction of the Ag–ZnO/Syltherm 800 hybrid nanofluid increases by 13.13%, 27.32%, 42.99%, and 50.56% for 1.0%, 2.0%, 3.0%, and 4.0% nanoparticle volume fractions, respectively, compared with the base fluid Syltherm 800. In addition, the influence of Reynolds number on the convection heat transfer coefficient is found to be significant. Similarly, the convection heat transfer coefficient increases with the increase of the Reynolds number in all hybrid nanofluid types. The reason for this condition is the formation of a thinner boundary layer with the increase of Reynolds number. Also, at higher Reynolds numbers the receiver bulk temperature and wall temperature are lower. On the other hand, it can be seen from the rapid increase in Fig. 6 that the impact of the nanoparticle fraction is higher with rising Reynolds number.

Figure 7 shows the percentage effect of Ag–ZnO/Syltherm 800, Ag–TiO_2/Syltherm 800, and Ag–MgO/Syltherm 800 hybrid nanofluid types and their various nanoparticle volume fractions on the convection heat transfer coefficient. The goal of this graph is to make the apparent values of Ag–TiO_2/Syltherm 800, and Ag–MgO/Syltherm 800 hybrid nanofluids. These percent increases are relative to Syltherm 800. In general, it can be noticed that the Ag–MgO/Syltherm 800 hybrid nanofluid increases the convection heat transfer coefficient further. The increase in the convection heat transfer coefficient with the increasing nanoparticle volume fraction is approaching 50%. The lowest increase is approximately 10% in Ag–ZnO/Syltherm 800 hybrid nanofluid having the nanoparticle volume fraction of 1.0%.

Figure 8 shows the Nusselt number distribution for the base fluid Syltherm 800 base fluid, and Ag–ZnO/Syltherm 800, Ag–TiO_2/Syltherm 800, and Ag–MgO/Syltherm 800 hybrid nanofluids depending on the Reynolds number and

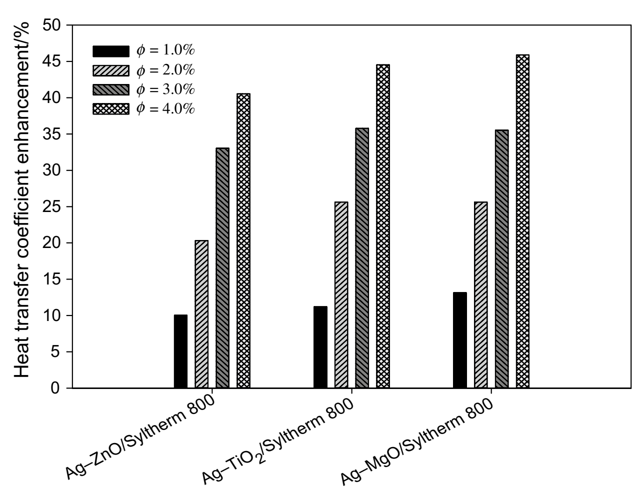

Fig. 7 Enhancement of convection heat transfer coefficient for different hybrid nanofluids

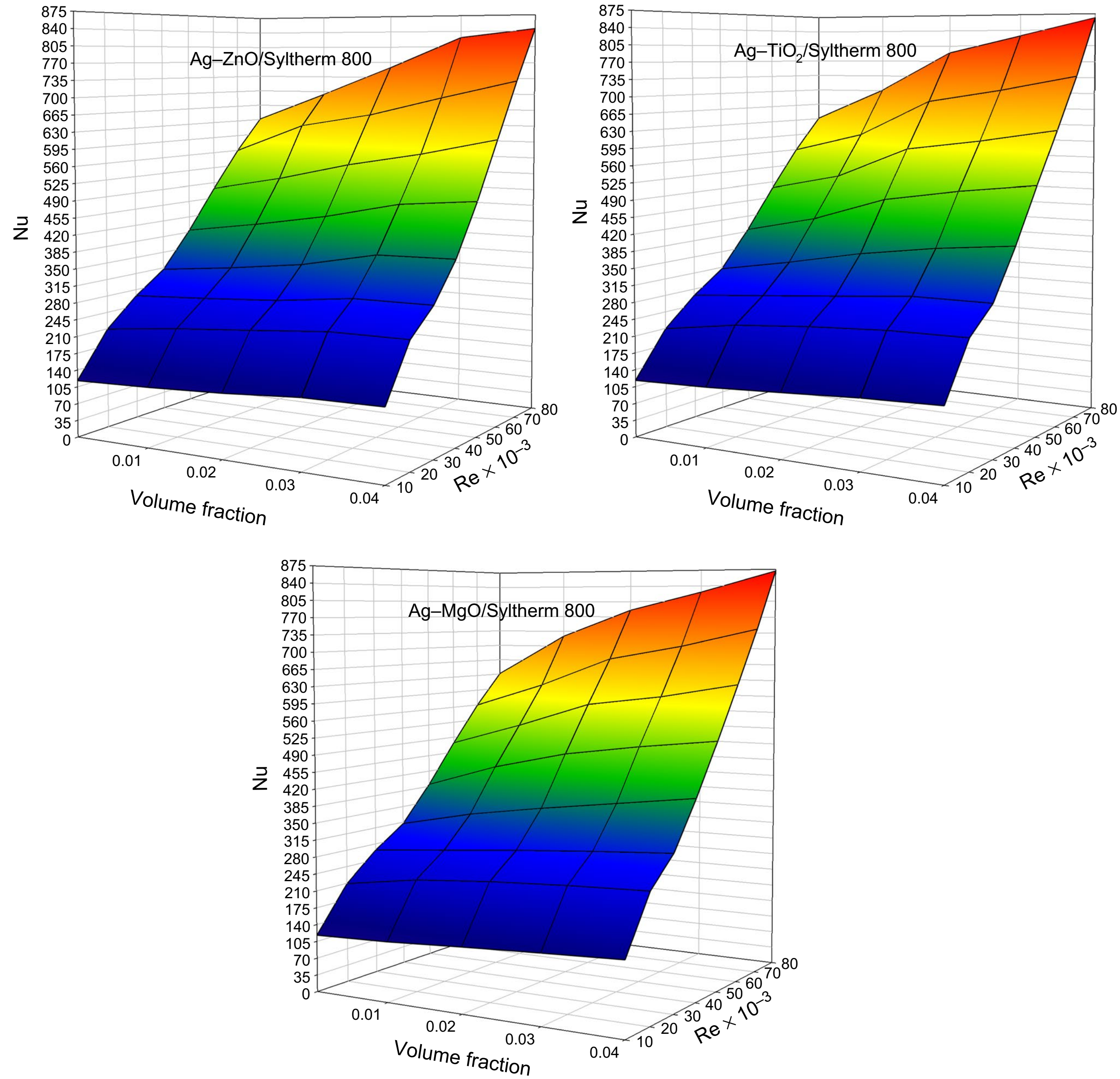

Fig. 8 Variations of Nusselt number for different hybrid nanofluid types in respect to nanoparticle volume fraction and Reynolds number

nanoparticle volume fraction. As can be seen, in all hybrid nanofluid types, Nusselt numbers increase with increasing nanoparticle volume fraction and Reynolds number. Ag–TiO_2/Syltherm 800, and Ag–MgO/Syltherm 800 hybrid nanofluids are found to have close Nusselt number values. It can be seen in Fig. 9 for a better understanding of this difference. The graphs have the same characteristic as Fig. 6.

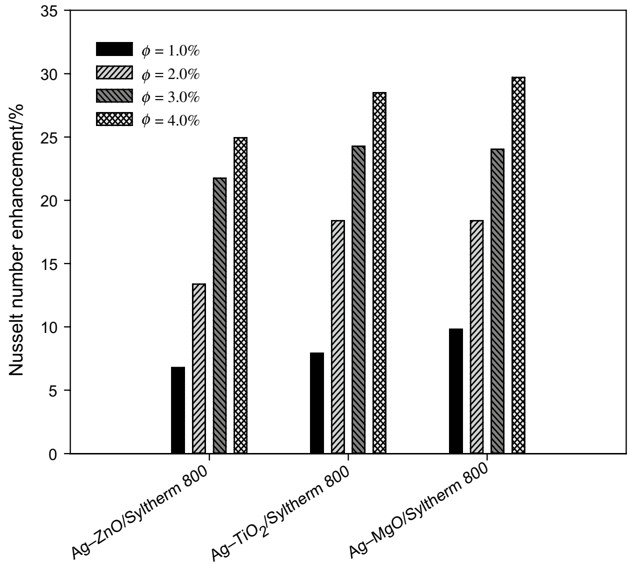

Fig. 9 Enhancement of Nusselt number for different hybrid nanofluid types with different nanoparticle volume fractions

The percentage increase in the Nusselt number for different hybrid nanofluid types in the study is shown in Fig. 9. The increases in this graph indicate the average increment according to the Nusselt number values of Syltherm 800. Also, Nusselt number increment values of the Ag–MgO/Syltherm 800 hybrid nanofluid increase in all nanoparticle volume fractions more than other the hybrid nanofluids. This value reaches about 30% for Ag–MgO/Syltherm 800 hybrid nanofluid with a 4.0% nanoparticle volume fraction.

The changing of friction factors with Reynolds number for the base fluid of Syltherm 800, Ag–ZnO/Syltherm 800, Ag–TiO_2/Syltherm 800, and Ag–MgO/Syltherm 800 hybrid nanofluids is given in Fig. 10. It can be deduced from the graphs how the friction factor affects the use of different hybrid nanofluids, various volume fractions of nanoparticle, and Reynolds numbers. As it is known, shear viscosity of nanofluid increases with adding nanoparticles so that raise the viscosity [58] and the density of the fluid. This condition increases the flow friction in the fluid and requires

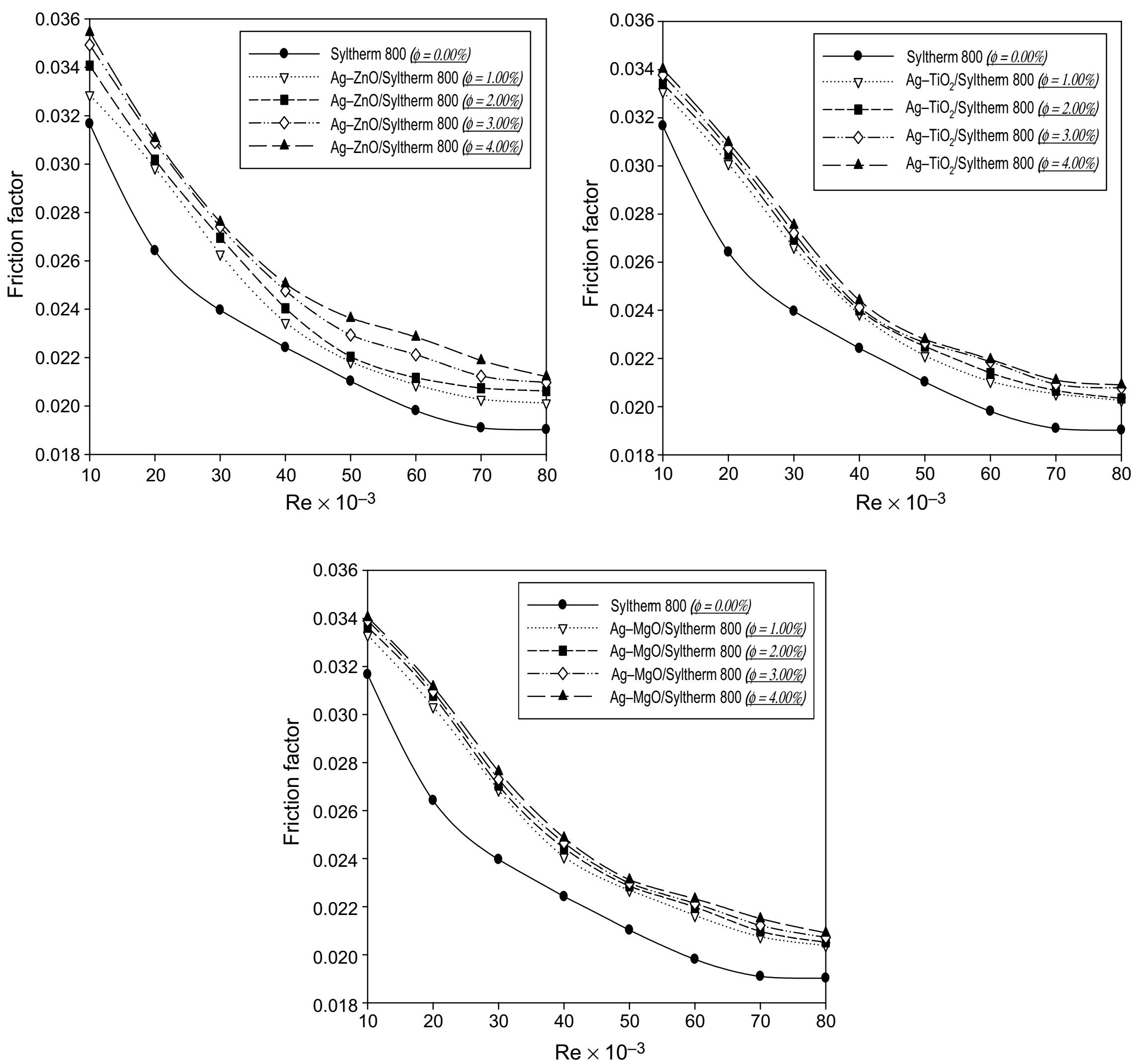

Fig. 10 Variations of friction factor in terms of nanoparticle volume fraction and Reynolds number for different hybrid nanofluid types

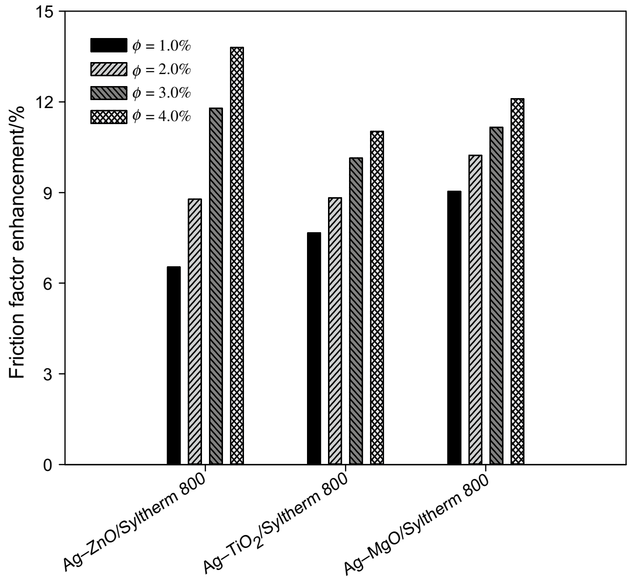

Fig. 11 Increment of friction factor for different hybrid nanofluids

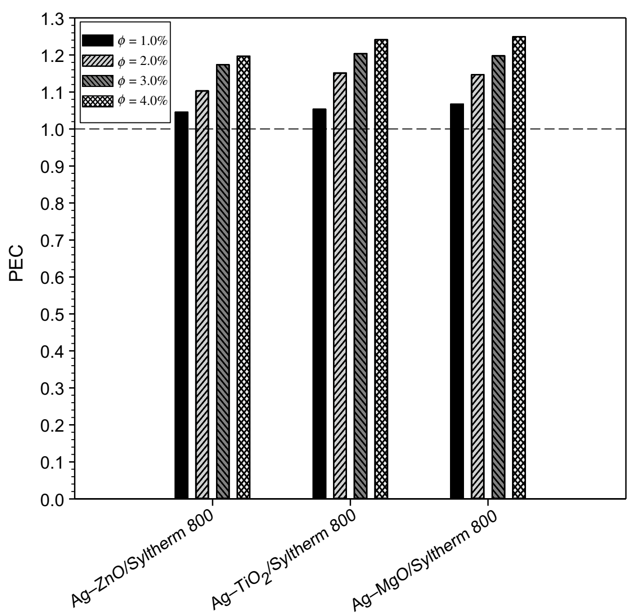

Fig. 12 PEC number for different hybrid nanofluid with different nanoparticle volume fractions

higher pumping power. When the graphs are examined, it can be revealed that the friction factor decreases due to the growth of the Reynolds number for all of the fluids used in the PTC receiver. It is noticed that the differences between the friction factors of hybrid nanofluids and Syltherm 800 are greater. In other words, using the hybrid nanofluids visibly increases the friction factor relative to the base fluid. However, when the friction factor of hybrid nanofluids is examined, it can be noticed that the differences between values of friction factor are so small. In addition, since the nanoparticle volume fraction increases for all types of hybrid nanofluids, the friction factor naturally increases, too.

Figure 11 is a graph that shows the effect of using hybrid nanofluids with different nanoparticle volume fractions on the percentage friction factor compared to Syltherm 800. This graph is obtained by averaging the friction factors in all Reynolds numbers. It is generally desirable that the friction factors of the fluids used are low. From Fig. 11, it can be said that the friction factor of Ag–ZnO/Syltherm 800 nanofluid type with 4.0 nanoparticle volume fraction increases about 15% compared to Syltherm 800. Increment of the friction factor for Ag–TiO_2/Syltherm 800 and Ag–MgO/Syltherm 800 hybrid nanofluids is approximately similar. This is an advantage. Because these hybrid nanofluids have better heat transfer capabilities than Ag–ZnO/Syltherm 800.

Figure 12 shows the effect of different hybrid nanofluids and their several volume fractions of nanoparticle on PEC numbers. In the previous sections, it has been mentioned that the hybrid nanofluids increase both heat transfer and friction factor. The PEC number should be checked to see if the heat transfer or friction factor is dominant [52]. If PEC is greater than 1, heat transfer is dominant; if it is less than 1, the friction factor is dominant. In light of this information, the first thing that stands out in the graph is the PEC number of all hybrid nanofluids greater than 1. In other words, it can be inferred that all hybrid nanofluids have contributed to heat transfer by defeating the friction factor in comparison with Syltherm 800. It is noticed that the PEC number increases with the growth of nanoparticle volume fraction. For instance, the increase in PEC number at 1.0%, 2.0%, 3.0% and 4.0% nanoparticle volume fraction of Ag–ZnO/Syltherm 800, which increases heat transfer at least, is about 5%, 10%, 17% and 19%, respectively. The increase in PEC number at 1.0%, 2.0%, 3.0% and 4.0% nanoparticle volume

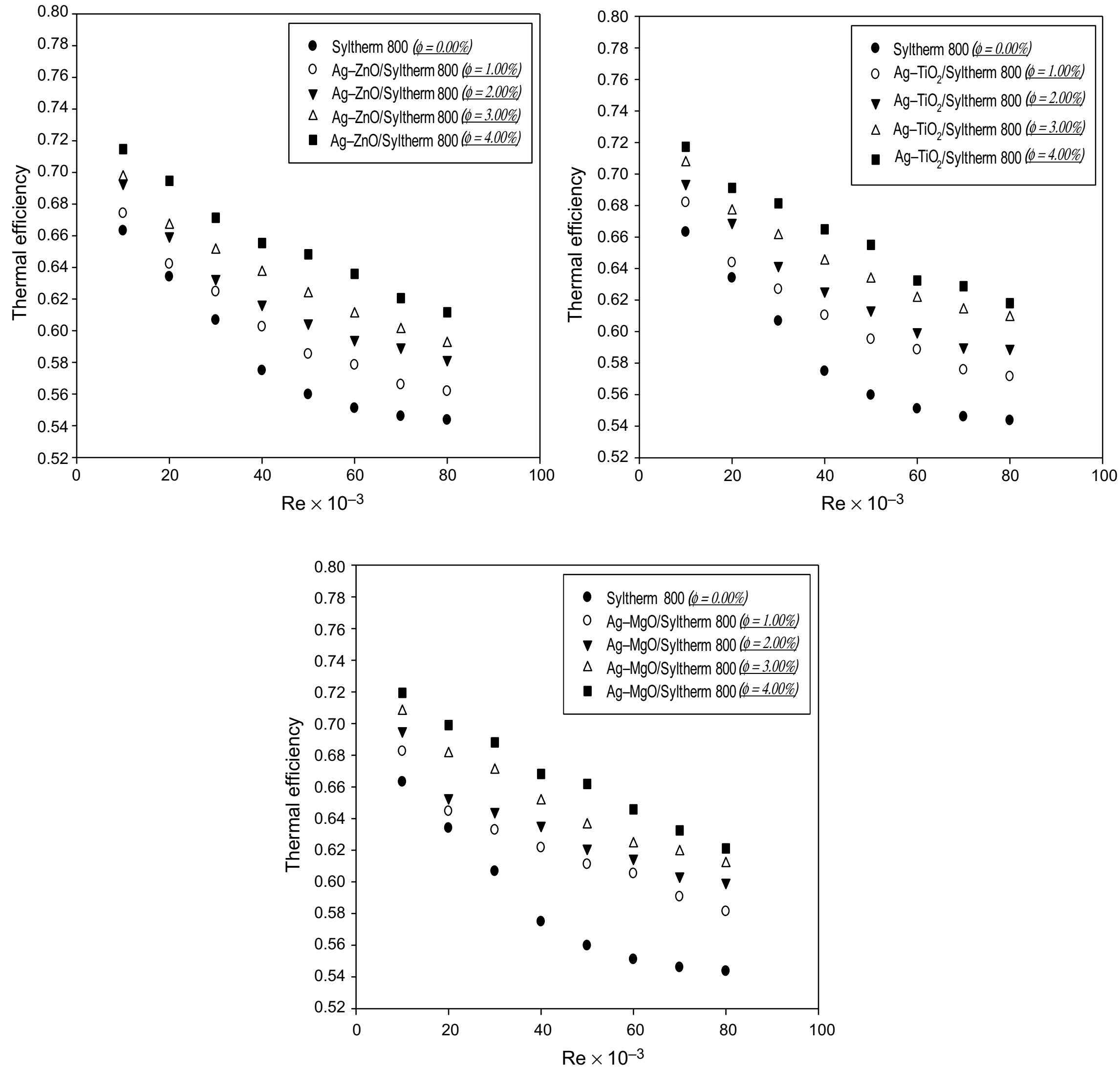

Fig. 13 Variations of thermal efficiency regarding volume fraction of nanoparticle and Reynolds number for different hybrid nanofluid types

fraction of Ag–MgO/Syltherm 800, which increases heat transfer the most, is about 6%, 14%, 19% and 25%, respectively. Furthermore, it can be observed that the PEC number values of Ag–TiO_2/Syltherm 800 and Ag–MgO/Syltherm 800 are close to each other.

Figure 13 shows the effect of Reynolds number on the thermal efficiency of the base fluid and different types of hybrid nanofluids and their nanoparticle volume fractions. In a sense, thermal efficiency is a measure of how much solar radiation benefits the system. In all fluids, it is observed that thermal efficiency decreases due to the increment in Reynolds number. The reason for this can be interpreted as the increment of pumping power with the growth of the Reynolds number. Thermal efficiency rises as the volume fraction of nanoparticles rises. Ag–MgO/Syltherm 800 increases thermal efficiency mostly. The smallest efficiency increment is observed for Ag–ZnO/Syltherm 800 hybrid nanofluid.

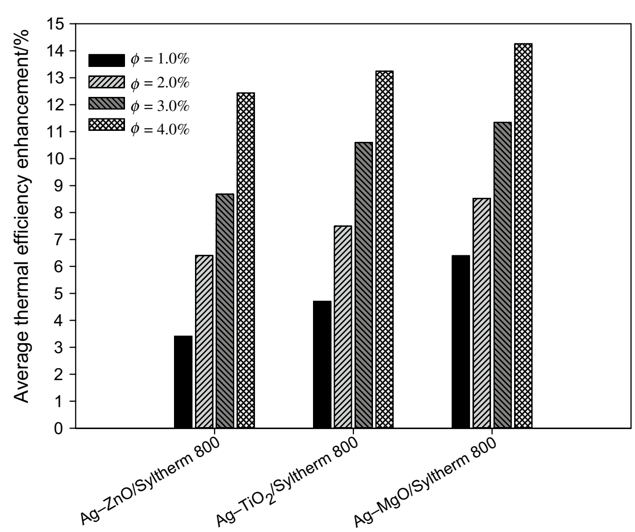

Fig. 14 Increment of thermal efficiency for different hybrid nanofluids

Fig. 15 Temperature contours of different hybrid nanofluid types at the receiver outlet

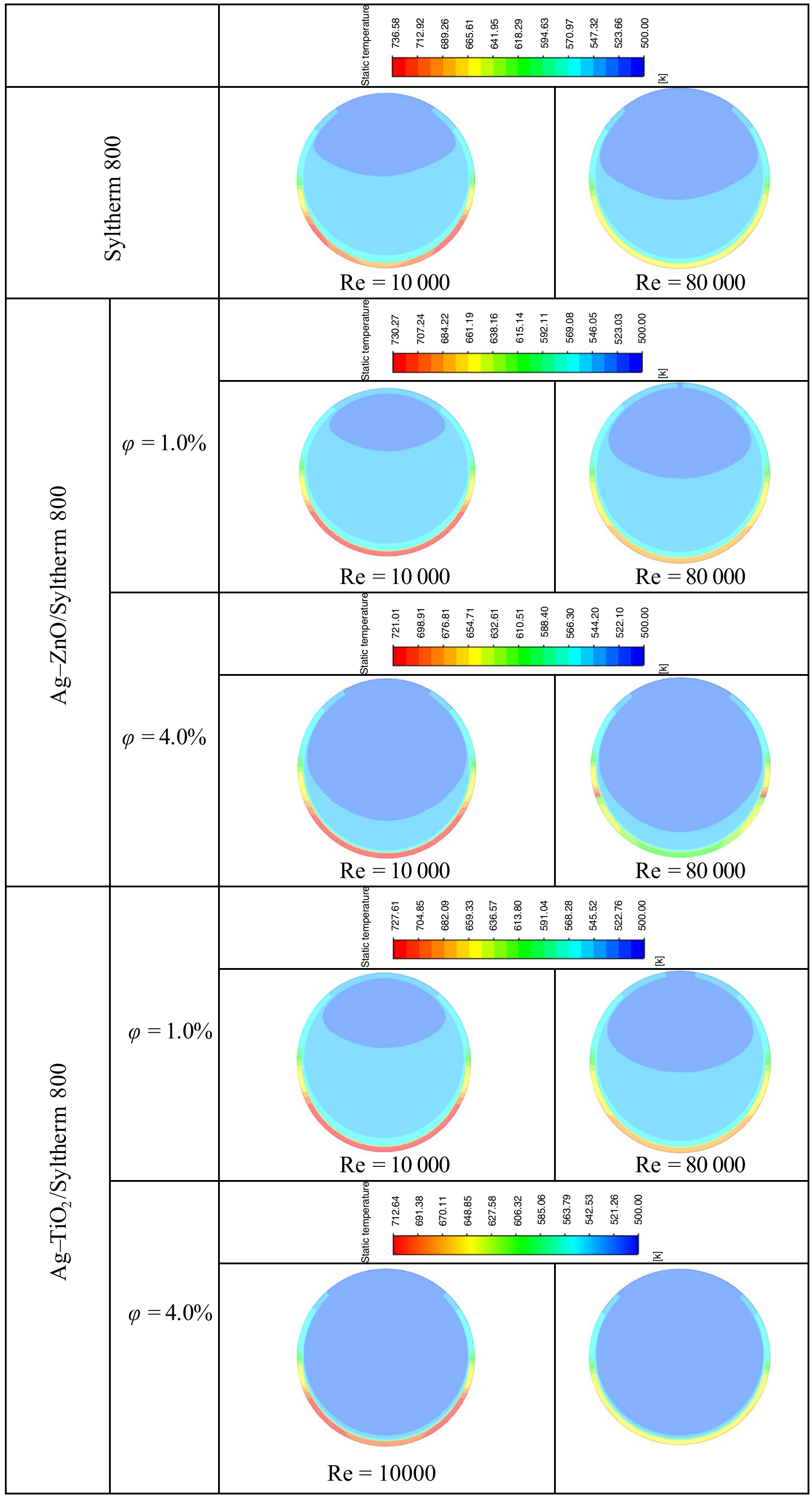

Fig. 15 (continued)

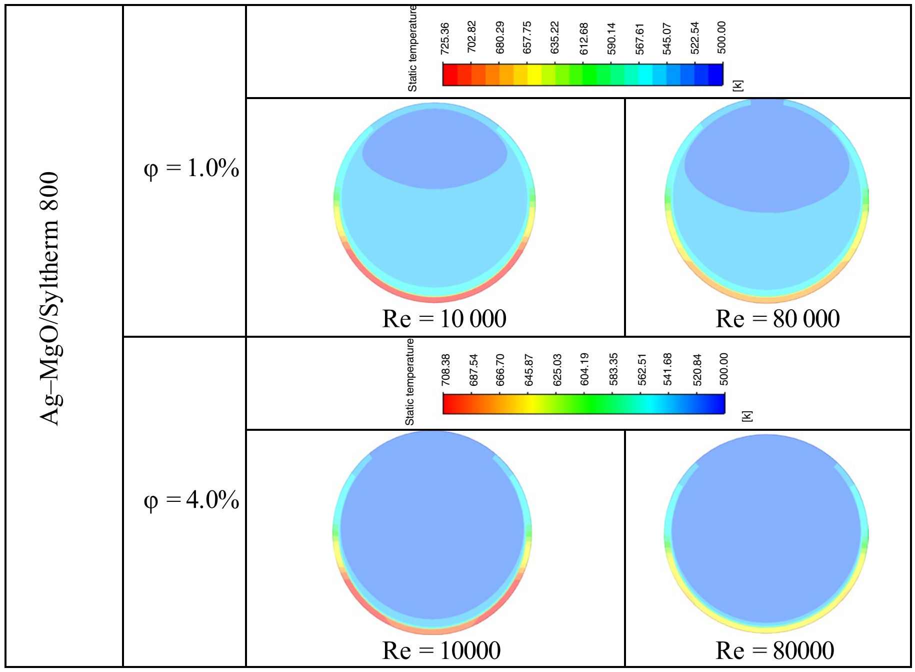

The change in percentage increment in average thermal efficiency is given in Fig. 14 for the Ag–ZnO/Syltherm 800, Ag–TiO_2/Syltherm 800, and Ag–MgO/Syltherm 800 hybrid nanofluid types. The changes in this graph are found compared with the Syltherm 800 fluid. Ag–MgO/Syltherm 800 is obtained to increase thermal efficiency by up to 15%. The friction factor values of this nanofluid are also reasonable compared to other hybrid nanofluids. This nanofluid can be predicted to be the best fluid to use for PTC. The effect of nanoparticle volume fraction on thermal efficiency seems to be great. For example, if the Ag–MgO/Syltherm 800 hybrid nanofluid is used with 1.0%, 2.0% and 3.0% nanoparticle volume fractions instead of Syltherm 800, the increment would be 6%, 8%, and 11%, respectively.

Figure 15 represents the temperature contours of the Syltherm 800 base fluid, Ag–ZnO/Syltherm 800, Ag–TiO_2/Syltherm 800, and Ag–MgO/Syltherm 800 hybrid nanofluids at the receiver outlet for 1.0% and 4.0% nanoparticle volume fraction and Re = 10,000 and Re = 80,000. It is understood from the graphs that the Reynolds number and nanoparticle volume fraction are effective in temperature distribution. As the Reynolds number and volume fraction of nanoparticle rise, the temperature distribution in the fluid and the receiver wall becomes more uniform. We can determine this by decreasing the number of colors showing the temperature distribution. The temperature distribution in the receiver is highly effective in the deformation of the receiver. Accordingly, in terms of all properties (heat and flow characteristics), the Ag–MgO/Syltherm 800 hybrid nanofluid with 4.0% nanoparticle volume fraction and Re = 80,000 stands out as a step forward.

Conclusions

In this article, the effect of three different hybrid nanofluid types (Ag–ZnO/Syltherm 800, Ag–TiO_2/Syltherm 800, and Ag–MgO/Syltherm 800) with four different nanoparticle volume fractions ($\phi = 1.0$–4.0%) on the collector efficiency is numerically discussed by considering three-dimensional turbulent flow conditions for in the PTC receiver. The results of the numerical study can be compiled as follows:

1. The use of different hybrid nanofluid types has provided a great advantage in terms of convective heat transfer inside the PTC. It is noticed that convective heat transfer is enhanced by approximately 26%, 29%, and 31% when using 4.0 vol% Ag–ZnO/Syltherm 800, 4.0 vol% Ag–TiO_2/Syltherm 800, and 4.0 vol% Ag–MgO/Syltherm 800 hybrid nanofluid types instead of base fluid of Syltherm 800.
2. As the volume fraction of nanoparticles increases, the convective heat transfer enhances, too.
3. The friction factor increases with the using of hybrid nanofluids. It is noticed that the hybrid nanofluid of Ag–ZnO/Syltherm 800 increases the friction factor at the highest amounts, while Ag–MgO/Syltherm 800 increases it in the lowest amounts. This is an advantage for the Ag–MgO/Syltherm 800. Moreover, the friction factor increases up to about 15% with the increment in the volume fraction of nanoparticles.
4. The thermal efficiency, which shows how much the system benefits from solar radiation, has increased sig-

nificantly with the use of hybrid nanofluids. It is determined that the effect of 4.0 vol% Ag–MgO/Syltherm 800 hybrid nanofluid has the highest thermal efficiency than the other fluids. Thermal efficiency tends to decrease with increasing pumping power at higher Reynolds numbers.

5. Heat transfer performance of hybrid nanofluids is superior in comparison with their friction factor due to the PEC number is greater than 1.
6. When the results are evaluated, it can be concluded that the most suitable working fluid for PTC is Ag–MgO/Syltherm 800.

References

1. Bellos E, Tzivanidis C. Enhancing the performance of evacuated and non-evacuated parabolic trough collectors using twisted tape inserts, perforated plate inserts and internally finned absorber. Energies. 2018;11:1129.
2. Kumaresan G, Sudhakar P, Santosh R, Velraj R. Experimental and numerical studies of thermal performance enhancement in the receiver part of solar parabolic trough collectors. Renew Sustain Energy Rev. 2017;77:1363–74.
3. Mahian O, Kianifar A, Kalogirou SA, Pop I, Wongwises S. A review of the applications of nanofluids in solar energy. Int J Heat Mass Transf. 2013;57:582–94.
4. Xuan Y, Li Q. Heat transfer enhancement of nanofluids. Int J Heat Fluid Flow. 2000;21:58–64.
5. Sajid MU, Ali HM. Thermal conductivity of hybrid nanofluids: a critical review. Int J Heat Mass Transf. 2018;126:211–34.
6. Mahian O, Kianifar A, Sahin AZ, Wongwises S. Entropy generation during Al_2O_3/water nanofluid flow in a solar collector: effects of tube roughness, nanoparticle size, and different thermophysical models. Int J Heat Mass Transf. 2014;78:64–75.
7. Sajid MU, Ali HM, Sufyan A, Rashid D, Zahid SU, Rehman WU. Experimental investigation of TiO_2–water nanofluid flow and heat transfer inside wavy mini-channel heat sinks. J Therm Anal Calorim. 2019;137:1279–94.
8. Shahsavar A, Saghafian M, Salimpour MR, Shafii MB. Effect of temperature and concentration on thermal conductivity and viscosity of ferrofluid loaded with carbon nanotubes. Heat Mass Transf. 2016;52:2293–301.
9. Shahsavar A, Salimpour MR, Saghafian M, Shafii MB. An experimental study on the effect of ultrasonication on thermal conductivity of ferrofluid loaded with carbon nanotubes. Thermochim Acta. 2015;617:102–10.
10. Shahsavar A, Salimpour MR, Saghafian M, Shafii MB. Effect of magnetic field on thermal conductivity and viscosity of a magnetic nanofluid loaded with carbon nanotubes. J Mech Sci Technol. 2016;30:809–15.
11. Shahsavar A, Saghafian M, Salimpour MR, Shafii MB. Experimental investigation on laminar forced convective heat transfer of ferrofluid loaded with carbon nanotubes under constant and alternating magnetic fields. Exp Therm Fluid Sci. 2016;76:1–11.
12. Wahab A, Hassan A, Qasim MA, Ali HM, Babar H, Sajid MU. Solar energy systems—potential of nanofluids. J Mol Liq. 2019;289:111049.
13. Ali H, Babar H, Shah T, Sajid M, Qasim M, Javed S. Preparation techniques of TiO_2 nanofluids and challenges: a review. Appl Sci. 2018;8:587.
14. Amina B, Miloud A, Samir L, Abdelylah B, Solano JP. Heat transfer enhancement in a parabolic trough solar receiver using longitudinal fins and nanofluids. J Therm Sci. 2016;25:410–7.
15. Bretado de los Rios MS, Rivera-Solorio CI, García-Cuéllar AJ. Thermal performance of a parabolic trough linear collector using Al_2O_3/H_2O nanofluids. Renew Energy. 2018;122:665–73.
16. Ghasemi SE, Ranjbar AA. Thermal performance analysis of solar parabolic trough collector using nanofluid as working fluid: a CFD modelling study. J Mol Liq. 2016;222:159–66.
17. Kaloudis E, Papanicolaou E, Belessiotis V. Numerical simulations of a parabolic trough solar collector with nanofluid using a two-phase model. Renew Energy. 2016;97:218–29.
18. Khakrah H, Shamloo A, Kazemzadeh HS. Determination of parabolic trough solar collector efficiency using nanofluid: a comprehensive numerical study. J Sol Energy Eng. 2017;139:051006.
19. Mwesigye A, Huan Z, Meyer JP. Thermodynamic optimisation of the performance of a parabolic trough receiver using synthetic oil–Al_2O_3 nanofluid. Appl Energy. 2015;156:398–412.
20. Mwesigye A, Huan Z, Meyer JP. Thermal performance and entropy generation analysis of a high concentration ratio parabolic trough solar collector with Cu-Therminol®VP-1 nanofluid. Energy Convers Manag. 2016;120:449–65.
21. Alsarraf J, Rahmani R, Shahsavar A, Afrand M, Wongwises S, Tran MD. Effect of magnetic field on laminar forced convective heat transfer of MWCNT–Fe_3O_4/water hybrid nanofluid in a heated tube. J Therm Anal Calorim. 2019;137:1809–25.
22. Shahsavar A, Godini A, Sardari PT, Toghraie D, Salehipour H. Impact of variable fluid properties on forced convection of Fe_3O_4/CNT/water hybrid nanofluid in a double-pipe mini-channel heat exchanger. J Therm Anal Calorim. 2019;137:1031–43.
23. Shahsavar A, Sardari PT, Toghraie D. Free convection heat transfer and entropy generation analysis of water–Fe_3O_4/CNT hybrid nanofluid in a concentric annulus. Int J Numer Methods Heat Fluid Flow. 2019;29:915–34.
24. Hemmat Esfe M, Alirezaie A, Rejvani M. An applicable study on the thermal conductivity of SWCNT–MgO hybrid nanofluid and price-performance analysis for energy management. Appl Therm Eng. 2017;111:1202–10.
25. Minea AA. Challenges in hybrid nanofluids behavior in turbulent flow: recent research and numerical comparison. Renew Sustain Energy Rev. 2017;71:426–34.
26. Minea AA. Hybrid nanofluids based on Al_2O_3, TiO_2 and SiO_2: numerical evaluation of different approaches. Int J Heat Mass Transf. 2017;104:852–60.
27. Moghadassi A, Ghomi E, Parvizian F. A numerical study of water based Al_2O_3 and Al_2O_3–Cu hybrid nanofluid effect on forced convective heat transfer. Int J Therm Sci. 2015;92:50–7.
28. Chamkha AJ, Miroshnichenko IV, Sheremet MA. Numerical analysis of unsteady conjugate natural convection of hybrid water-based nanofluid in a semicircular cavity. J Therm Sci Eng Appl. 2017;9:041004-1.
29. Nabil MF, Azmi WH, Hamid KA, Zawawi NNM, Priyandoko G, Mamat R. Thermo-physical properties of hybrid nanofluids and hybrid nanolubricants: a comprehensive review on performance. Int Commun Heat Mass Transf. 2017;83:30–9.
30. Sidik NAC, Adamu IM, Jamil MM, Kefayati GHR, Mamat R, Najafi G. Recent progress on hybrid nanofluids in heat transfer applications: a comprehensive review. Int Commun Heat Mass Transf. 2016;78:68–79.
31. Minea AA, El-Maghlany WM. Influence of hybrid nanofluids on the performance of parabolic trough collectors in solar thermal

systems: recent findings and numerical comparison. Renew Energy. 2018;120:350–64.
32. Bellos E, Tzivanidis C. Thermal analysis of parabolic trough collector operating with mono and hybrid nanofluids. Sustain Energy Technol Assess. 2018;26:105–15.
33. Nohavica D, Gladkov P. ZnO nanoparticles and their applications-new achievements, Olomouc, Czech Republic. EU 2010;10:12–14
34. Leena M, Srinivasan S. Synthesis and ultrasonic investigations of titanium oxide nanofluids. J Mol Liq. 2015;206:103–9.
35. Menlik T, Sözen A, Gürü M, Öztaş S. Heat transfer enhancement using MgO/water nanofluid in heat pipe. J Energy Inst. 2015;88:247–57.
36. Behar O, Khellaf A, Mohammedi K. A novel parabolic trough solar collector model—validation with experimental data and comparison to engineering equation solver (EES). Energy Convers Manag. 2015;106:268–81.
37. Fernández-García A, Zarza E, Valenzuela L, Pérez M. Parabolic-trough solar collectors and their applications. Renew Sustain Energy Rev. 2010;14:1695–721.
38. Forristall R. Heat transfer analysis and modeling of a parabolic trough solar receiver implemented in engineering equation solver [Internet]. 2003 Oct. Report No.: NREL/TP-550-34169, 15004820. http://www.osti.gov/servlets/purl/15004820/.
39. Bellos E, Tzivanidis C, Tsimpoukis D. Thermal enhancement of parabolic trough collector with internally finned absorbers. Sol Energy. 2017;157:514–31.
40. Mwesigye A, Bello-Ochende T, Meyer JP. Heat transfer and thermodynamic performance of a parabolic trough receiver with centrally placed perforated plate inserts. Appl Energy. 2014;136:989–1003.
41. Gong X, Wang F, Wang H, Tan J, Lai Q, Han H. Heat transfer enhancement analysis of tube receiver for parabolic trough solar collector with pin fin arrays inserting. Sol Energy. 2017;144:185–202.
42. Kurşun B. Thermal performance assessment of internal longitudinal fins with sinusoidal lateral surfaces in parabolic trough receiver tubes. Renew Energy. 2019;140:816–27.
43. Ansys fluent 19 theory guide pdf [Internet]. [cited 2019 Sep 19]. http://drawer.ne.jp/wordpress/wp-content/uploads/2019/08/5cxu/ansys-fluent-19-theory-guide-pdf.html.
44. Versteeg HK, Malalasekera W. An introduction to computational fluid dynamics: the finite volume method. London: Pearson Education; 2007.
45. https://thermtest.com/materials-database#.
46. Pak BC, Cho YI. Hydrodynamic and heat transfer study of dispersed fluids with submicron metallic oxide particles. Exp Heat Transf. 1998;11:151–70.
47. Tayebi T, Chamkha AJ. Free convection enhancement in an annulus between horizontal confocal elliptical cylinders using hybrid nanofluids. Numer Heat Transf Part Appl. 2016;70:1141–56.
48. Brinkman HC. The viscosity of concentrated suspensions and solutions. J Chem Phys. 1952;20:571–571.
49. Maxwell JC. A treatise on electricity and magnetism. Oxford: Clarendon Press; 1881.
50. Wang P, Liu DY, Xu C. Numerical study of heat transfer enhancement in the receiver tube of direct steam generation with parabolic trough by inserting metal foams. Appl Energy. 2013;102:449–60.
51. Huang Z, Li Z-Y, Yu G-L, Tao W-Q. Numerical investigations on fully-developed mixed turbulent convection in dimpled parabolic trough receiver tubes. Appl Therm Eng. 2017;114:1287–99.
52. Ekiciler R, Arslan K. CuO/water nanofluid flow over microscale backward-facing step and heat transfer performance analysis. Heat Transf Res. 2018;49:1489–505.
53. Cheng ZD, He YL, Cui FQ. Numerical study of heat transfer enhancement by unilateral longitudinal vortex generators inside parabolic trough solar receivers. Int J Heat Mass Transf. 2012;55:5631–41.
54. Dittus FW, Boelter LMK. Heat transfer in automobile radiators of tubular type. Berkeley: University of California Press; 1930.
55. Gnielinski V. New equations for heat and mass transfer in turbulent pipe and channel flow. Int Chem Eng. 1976;16:359–68.
56. Petukhov BS. Heat transfer and friction in turbulent pipe flow with variable physical properties. Adv Heat Transf. 1970;6:503–64.
57. Blasius PRH. Das Aehnlichkeitsgesetz bei Reibungsvorgangen in Flüssigkeiten. Forschungsheft. 1913;1–41.
58. Jabbari F, Rajabpour A, Saedodin S. Viscosity of carbon nanotube/water nanofluid. J Therm Anal Calorim. 2019;135:1787–96.

Publisher's Note Springer Nature remains neutral with regard to jurisdictional claims in published maps and institutional affiliations.